Revision1

Elastic wave velocity anomalies of anorthite in subducting plate: In situ experiments

Kyoko N. Matsukage[1,*], Yu Nishihara[2], Fumiya Noritake[3], Katsuyuki Kawamura[3], Noriyoshi Tsujino[4], Moe Sakurai[5], Yuji Higo[6], Junichi Nakajima[7], Akira Hasegawa[7] and Eiichi Takahashi[5]

[1]Earth and Planetary Sciences, Kobe University, Rokkoudai, Nada-ku, Kobe 657-8501, Japan
[2]Geodynamics Research Center, Ehime University, Bunkyocho, Matsuyama, Ehime 790-8577, Japan
[3]Environmental Science and Technology, Okayama University, Tsushimanaka, Kita, Okayama 700-8530, Japan
[4]Institute for Study of the Earth's Interior, Okayama University, Okayama, Japan
[5]Earth and Planetary Sciences, Tokyo Institute of Technology, Ookayama, Meguro-ku, Tokyo 152-8551, Japan
[6]Japan Synchrotron Radiation Research Institute, Hyogo 679-5198, Japan
[7]Research Center for Prediction of Earthquakes and Volcanic Eruptions, Graduate School of Science, Tohoku University, Sendai 980-8578, Japan

*Corresponding author: K.N. Matsukage,
E-mail: kmatsu@people.kobe-u.ac.jp

Submitted to American Mineralogist

25 **ABSTRACT**

26 To understand the origin of observed low-velocities in the crustal portion of subducting plates,
27 we performed in situ measurements of elastic wave velocities of anorthite at temperatures up
28 to 1373 K at pressure of ~1 GPa and up to 773 K at 2.0-7.0 GPa. A fine-grained
29 polycrystalline anorthite which was synthesized using a gas pressure apparatus was used for
30 the measurements. The high pressure experiments were performed using the multi-anvil
31 apparatus installed on beam-line BL04B1 at SPring-8. The elastic wave velocity was
32 measured by the ultrasonic pulse method with synchrotron X-ray radiographic imaging and
33 X-ray diffraction techniques. At ~1.0 GPa, elastic wave velocities exhibited a sharp
34 temperature-induced kink at ~500 K. Below 500 K, the elastic wave velocities decrease with
35 increasing temperature. In contrast, above 500 K, the elastic wave velocities show an
36 increasing trend in the range of 500-900 K, and then revert back to a decreasing trend at
37 above 900 K. We also found a pressure-induced velocity anomaly of anorthite. At 300-373 K,
38 V_P is constant up to 4 GPa, but decrease above 4 GPa with increasing pressure, while V_S
39 decreases monotonously with increasing pressure. These elastic anomalies is considered to be
40 attributable to the tilting behaviour of the corner-sharing TO_4 (T = Al, Si) tetrahedra in three
41 dimensional frameworks of anorthite. Our results suggest the presence of plagioclase feldspar
42 has the potential to causes low velocity anomaly in the subducting oceanic crust when it
43 survives as a metastable phase in the slab at higher pressure and lower temperature
44 conditions.

45

46 Keywords: anorthite, plagioclase, elastic wave velocities, subduction, oceanic crust

47

48

INTRODUCTION

Seismological observations have detected heterogeneous low-velocity structure in the crustal portion of subducting plates (e.g., Kawakatsu and Watada 2007; Rondenay et al. 2010). Plagioclase feldspars are one of the most abundant minerals in the crustal portion. Crusts with MORB-like composition contain large amount of plagioclase, normally more than 50 wt%. Therefore, the knowledge of the physical properties of plagioclase is important in order to resolve the detailed structure of the crust and crustal portions of subducted slabs based on such seismological observations. The purpose of our study is to determine the physical behaviour of anorthite ($CaAl_2Si_2O_8$, an end member of plagioclase), and to discuss the origin of the low-velocity layer in the crustal portion of subducting plates.

Elastic wave velocity of plagioclase minerals and rock aggregates has been measured using ultrasonic pulse technique (e.g., Ryzhova 1964; Wang et al. 1973; Liebermann and Ringwood 1976; Seront et al. 1993; Kono et al. 2008). Previous studies, however, encounter some experimental difficulties. In this technique, the elastic wave velocities are obtained from travel time and sample length. Thus, accurate measurement of the sample length is crucial for determining accurate elastic wave velocities (Li et al. 1998). In all previous studies for plagioclase, except for one study performed at room pressure (Ryzhova 1964), the sample lengths were not measured directly and were estimated by calculation using equation of state of minerals based on the assumption that only isotropic elastic deformation causes sample strain under high pressure and high temperature. In order to overcome this problem, synchrotron X-ray radiographic imaging technique has been applied in the elastic wave velocity measurements (Kung et al. 2002). When this method is used, direct measurement of the sample length in a high-pressure apparatus can be carried out. Recently, the experimental system for in situ ultrasonic measurement combined with X-ray radiographic imaging

technique has been installed at Spring-8, Japan (Higo et al. 2009). Here, we report the result of elastic wave velocity measurements on anorthite employing the ultrasonic pulse method under high pressure and high temperature with synchrotron X-ray radiographic imaging and X-ray diffraction techniques.

EXPERIMENTAL METHODS

Synthesis of polycrystalline anorthite

A polycrystalline anorthite was synthesised using the gas pressure apparatus installed at Tokyo Institute of Technology. The starting material was prepared from reagent grade SiO_2, Al_2O_3 and $CaCO_3$, which were mixed in an appropriate ratio and ground in an agate mortar and pestle with ethanol. The mixed sample was decarbonated in a 1-atm furnace at 1273 K for 24 hours. Then, it was melted at 1873 K and quenched to form glass. The glass sample was ground in ethanol and loaded into a sealed Pt tube container (3.0 mm inner diameter and 0.2 mm thickness). The sample was preheated at 1173 K for 2 hours, and then it was kept at 1373 K for 20 hours at pressure of 0.3 GPa. Figure 1a shows an orientation contrast image of the synthesised polycrystalline anorthite. The anorthite crystals are predominantly anhedral with mosaic texture, and some of crystals exhibit short columnar shape. The average grain size is less than 10 μm across. Orientations of grains in the polycrystalline anorthite are estimated to be random based on observation of a thin section under an optical microscope, which showed random extinction of transmitted polarized light. The bulk density of the synthesised anorthite measured by the Archimedes method is 2.72 ± 0.02 g/cm^3, which is 98.8% of the X-ray density (= porosity of 1.2%). The sample was formed into cylinders with 2.0 mm in diameter using ultrasonic cutter and ground to ~1.0 mm in length, and both ends of cylinder were polished with 1 μm diamond paste.

97

98 **In situ measurements of elastic wave velocities and X-ray diffraction**

99 In situ measurements of the elastic wave velocities (V_P and V_S) of anorthite were
100 performed at pressures between 0.6 and 7.0 GPa at temperatures of up to 1373 K. The
101 experiments were performed using the Kawai-type multi-anvil apparatus (SPEED-1500) on
102 beam-line BL04B1 at the synchrotron facility of Spring-8 (Utsumi et al., 1998). The
103 experimental design for *in situ* elastic wave velocity measurement using the ultrasonic
104 pulse-echo-overlap method at BL04B1 was presented by Higo et al. (2009). Pressure was
105 generated by eight 26-mm tungsten carbide anvils (Tungaloy F grade) with truncated edge
106 length of 11 mm. A Co-doped semi-sintered MgO octahedron with an 18-mm edge length was
107 used as the pressure medium (Figure 2). A graphite sleeve was used as the heater and was
108 inserted in a ZrO_2 thermal insulation sleeve with an MgO window for X-ray path to reduce
109 potential temperature gradients. The temperature gradient of sample was estimated as ~25
110 °C/mm at the maximum (Matsukage and Kawasaki 2014). The sample was enclosed in an
111 hBN sleeve container, and then placed in the central part (hot part) of the furnace. Platinum
112 foils (2.5 μm in thickness) were inserted on both side of the sample for the determination of
113 sample length using the X-ray radiographic imaging technique (Figure 3a). The precision of
114 the sample length measurement is estimated at 0.1-0.3 % of the nominal sample length (Higo
115 et al., 2009). An Al_2O_3 rod (5.3 mm in length and 2.0 mm in diameter) was used as the buffer
116 rod for transmitting ultrasonic waves to the sample. The ultrasonic signals were generated and
117 received by 10°Y-cut $LiNbO_3$ transducer having thickness of 50 μm and diameter of 3.2 mm.
118 We used ultrasonic waves at frequencies of 30-60 MHz for 3 cycles (Figures 3b and 3c).
119 The diffracted X-ray from the sample was measured simultaneously with the
120 measurement of elastic wave velocities. A solid-state detector connected to a multi-channel

analyzer combined with incident white X-ray beam was used for data collection. The multichannel analyzer was calibrated with the characteristic X-rays of Cu, Mo, Ag, Ta, Pt, Au and Pb. The X-ray diffractions were collected at a fixed 2θ angle (= 2.961°), which was determined using the unit-cell volume of MgO at room pressure and temperature. The incident X-ray beam was collimated to 0.2 and 0.1 mm in the vertical and horizontal dimensions, respectively. Slits of 2.0 mm in the vertical dimension and 0.1 mm in the horizontal dimension were used between the sample and the detector. MgO was used as a pressure marker, and it was mixed with hexagonal boron nitride (hBN) (MgO:hBN = 1:1 by weight) to prevent grain growth at high temperatures. Exposure times for collecting diffraction patterns of the sample and pressure marker were 300 and 180 s, respectively. Temperature was measured by a $W_{97}Re_3$-$W_{75}Re_{25}$ thermocouple. No pressure correction was made on the emf of the thermocouple. The pressure was calculated from the two diffraction peaks of MgO (111 and 200) using the equation of state of MgO presented by Jamieson et al. (1982) in program "XRayAna" available at the beam-line BL04B1.

RESULTS

The elastic wave velocities and X-ray diffraction measurements were carried out under pressures up to 7 GPa in a series of heating and cooling cycles (Table 1, Figure 4). First, we compressed the sample to ~2.0 GPa (load = 80 ton), then heated it to 1373 K where it was kept for 60 minutes at 1373 K under constant oil pressure (cycle (1)). The purpose of the first heating and cooling cycle is to relax the stress on the sample and its surrounding materials, and to obtain better mechanical contact between the buffer rod and sample. This compression and preheating process is important for obtaining reliable signals of elastic waves (e.g., Li et al. 2004). After preheating, V_P, V_S and X-ray diffraction measurements were performed in the

cooling stage of seven heating and cooling cycles (2)-(8). After each cooling stage, we increased the oil pressure, and then started the next heating and cooling cycle. The data of cycle (2) was collected up to 1373 K at *P*-*T* conditions where anorthite is thermodynamically stable (Hays 1966). The data of cycles (3)-(8) were collected up to 773 K at metastable conditions.

In this study, we found a kink in elastic wave velocities with discontinuous change in temperature dependence at a temperature of about 500 K in cycle (2) (Figure 5). Below 500 K, the elastic wave velocities decrease with increasing temperature. In contrast, above 500 K, the elastic wave velocities show an increasing trend in the range of 500-900 K, and then revert back to a decreasing trend at above 900 K. Kinks similar to that of cycle (2) is observed for the cycles (3)-(5). At these cycles, temperatures at the kinks increase with increasing pressure, from ~500 K to ~720 K. In the cycles (6)-(8), kinks are not apparent within the studied temperature ranges, and only a monotonously decreasing trend is observed with increasing temperature. Elastic wave velocity measurement of anorthite was performed twice, and the temperature-induced elastic anomalies which are described here were observed in both experiments (see appendix). We also found a pressure-induced velocity anomaly of anorthite (Figure 6). At temperature of 300-373 K, V_P decreases with increasing pressure at above 4 GPa, although it remains constant below 4 GPa. The V_S shows a decrease with increasing pressure. At 473 K, both V_P and V_S exhibit increasing trends below 4 GPa while showing a decreasing trend with increasing pressure above 4 GPa. At above 573 K, V_P and V_S decrease monotonously with increasing pressure up to 7 GPa.

All X-ray diffraction peaks correspond to anorthite with triclinic structure (Figure 7) (e.g., Foit and Peacor, 1973). For anorthite, the *P*(-1) structure is stable at ambient condition, and it changes to *I*(-1) structures with increasing temperature (e.g., Redfern and Salje 1987;

Redfern et al. 1988) and with increasing pressure (e.g., Angel 1988, 1992; Hackwell and Angel 1995) (Figure 4). Because there is no significant difference in the position of atoms between these structures, X-ray diffraction patterns resemble one another. Previous studies (e.g., Hackwell and Angel 1995; Tribaudino and Angel 2012) distinguished I(-1) phase from P(-1) by using the disappearance of 11(-1) reflection (c-type reflection: h + k = even, l = odd) that is absent in I(-1) phase due to the symmetry of body centered structure. In our experiments, 11(-1) reflection was observed at 300-473 K in cycle (2) and at ambient condition before and after the experiments. The X-ray diffraction patterns of sample exhibit no additional peaks at any of the pressure and temperature conditions, although a small amount of reaction products (< 1 %) were observed at the grain boundaries of anorthite crystals from the recovered sample (Figure 1b). Unit cell parameters and volume of the sample are determined by Le Bail method in program GSAS (Von Dreele and Larson 2001) using all diffraction lines shown in Figure 7. The unit cell parameters a, b, c, α and β decrease with increasing pressure and γ increase with increasing pressure (Figure 8). The change in temperature dependence of unit cell angles (β and γ) at about 500-550 K is observed in cycles (2) and (3). The unit cell volume at ambient pressure (V_0 = 1341 Å^3) agrees well with that of Tribaudino and Angel (2012) (V_0 = 1340.1 Å^3). The unit cell volume gradually decreases with increasing pressure, though a weak kink is observed at about 4 GPa (Figure 9).

The adiabatic bulk modulus (K_S) and shear modulus (G) are represented by the equations: $K_S = \rho(V_P^2 - V_S^2 \times 4/3)$ and $G = \rho V_S^2$, where ρ is density. To calculate the K_S and G from the velocities and density data, we obtained density from the equation, $\rho = (m\ Z/N_A) \times (1/V)$, where m, Z, N_A and V are formula weight, formula number (Z = 8 for anorthite), the Avogadro constant and unit cell volume, respectively. The calculated ρ, K_S and G are listed in Table 1. In cycles (2), (3) and (4), kinks of K_S and G are observed at ~500-750 K. Adiabatic

bulk modulus (= K_{S0}) and shear modulus (= G_0) at room temperature and room pressure were estimated by polynomial fitting using data at 300 K. We obtained K_{S0} = 83 GPa and G_0 = 38.6 GPa. Based on Angel's (2004) data on plagioclase feldspars, isothermal bulk modulus (K_{T0}) at ambient condition was estimated by Tribaudino et al. (2011) to be K_{T0} = 82.5 GPa. K_{S0} is calculated as 82.7 GPa from the formula $K_{S0} = K_{T0}(1 + \alpha\gamma T)$ where α and γ are thermal expansion coefficient and Grüneisen parameter, and are 1.379×10^{-5} K^{-1} and 0.46 (Tribaudino et al. 2011), respectively. The K_{S0} determined by our experiments is sufficiently consistent with those of previous study.

DISCUSSION AND CONCLUSIONS

Relationship with the phase transitions and the crystal structure

Anorthite is known for undergoing a reversible phase transition from $P(-1)$ to high-temperature $I(-1)$ at temperature of 510 K at pressures of less than ~2 GPa (e.g., Foit and Peacor 1973; Redfern et al. 1988). Temperature and pressure conditions of the discontinuous elasticity change at 500 K of cycle (2) agree well with the phase boundary of $P(-1)$ and high-temperature $I(-1)$ (Figure 4). Based on this observation, it is thought that anomalous behaviour at > 500 K is caused by successive structural changes in the high-temperature $I(-1)$ phase, followed by the phase transition. In our experiments, the temperature-induced anomaly is observed at higher pressure, at the P-T conditions near the extrapolated phase boundary by Hackwell and Angel (1995) (Figure 4). The structure of anorthite comprises a flexible three dimensional framework of rigid, corner sharing TO_4 tetrahedra (T = Si and Al) with Ca^{2+} occupying interstitial sites of the framework (e.g., Angel et al., 2013). Molecular dynamics (MD) simulation (Noritake et al. 2013) suggests that the temperature-induced anomalies of the K_S and G could be caused by a combination of two different thermal expansion

mechanisms due to atomic motions and displacements: (1) expansion of inter-atomic distances of near neighbor atoms and (2) increase in T-O-T angles of the framework. Below the phase transition temperature, thermal expansion is mainly caused by the expansion of the inter-atomic distances. In high-temperature $I(-1)$ stability field, two mechanisms contribute to the thermal expansion. The T-O-T angles increase with increasing temperature, which subsequently causes shortening of bridging bond length of T-O (e.g., Newton and Gibbs 1980) that contributes to increase in elastic moduli (K_S and G). This structural change in the $I(-1)$ stability field provides a reasonable explanation why the elastic wave velocities of anorthite increase with increasing temperature in the range of 500-900 K. Above 900 K, thermal expansion is dominated by the expansion of inter-atomic distance and results in the reduction of elasticity.

Angel (1992) performed single crystal X-ray diffraction experiments on five samples with various degrees of Al and Si cation disordering, and found that the pressure of phase transition from $P(-1)$ to high-pressure $I(-1)$ was dependent on the state of Si and Al order. When Q_{OD} (where Q_{OD} quantifies the state of order, varying from unity for complete Al and Si order to zero for complete disorder) decreases from 0.92 to 0.78, the pressure of the phase transition increases from 2.5 GPa to 4.8 GPa. In our sample, existence of the 11(-1) reflection seems to have suggested a possibility that the sample was ordered because the 11(-1) reflection should become less intense when the Q_{OD} decreases (Carpenter, 1991). However, for the synthesis method and condition of the anorthite in our study, it can be estimated that the state of Al and Si order should be partly disordered (Carpenter, 1991). The pressure condition of weak kink in the velocities and compression curves at ~4.0 GPa (Figures 6 and 9) is consistent with the phase boundary between $P(-1)$ and high-pressure $I(-1)$ for partly disordered anorthite for $Q_{OD} \cong 0.8$. The unit cell angles of α and γ are known to be sensitive to

241 the state of order, and the partly disordered anorthite ($Q_{OD} \cong 0.7$-0.8) has unit cell angles α =
242 93.2° and γ = 91.2° (Carpenter 1991; Angel 1992). At ambient condition, the sample used in
243 this study has α = 93.1° and γ = 91.2° which are quite consistent with that of previous studies
244 for the partly disordered anorthite. Consequently, we conclude that the anorthite sample in the
245 ultrasonic measurements is possible to be partly disordered and the kink of slope at ~4 GPa is
246 caused by the phase transition.

247 The velocities decrease accompanying pressure increase was observed in wide
248 pressure and temperature conditions of the experiments at above 4 GPa where *I*(-1) structures
249 are stable (Figure 6). This pressure-induced velocities anomaly (with the negative pressure
250 dependence) is in contrast to the positive effect for typical minerals such as olivine (e.g.,
251 Birch 1961, 1963). First, it is considered a possibility that the anomaly is an experimental
252 artefact originated by an influence of differential stress. The pressure increment induces a
253 differential stress in the sample, and the stress may influence to the elasticity. In this study, a
254 soft material (hBN) was used as the sample container to minimize the differential stress at the
255 compression, and the measurements were performed after heating to reduce the stress. Based
256 on the in situ X-ray diffraction measurements, the reduction of the stress was observed in the
257 sample and pressure maker at the heating. Consequently the influence of the differential stress
258 to the elasticity was not large in our experiments, and we considered that the pressure induced
259 anomaly is not an experimental artefact. Here, we suggest that the pressure induced anomaly
260 with the negative pressure dependence is caused by the tilting behavior of T-O-T angles in the
261 network of TO_4 tetrahedra. The MD simulation indicated that the average T-O-T angle of
262 anorthite decreases with increasing pressure, and this structural behaviour happens especially
263 at the high-temperature phase and the high-pressure phase with *I*(-1) symmetry (Noritake et al.
264 2013, 2014). When the T-O-T angle decrease and hence bridging bond length of T-O increase

with increasing pressure, elastic wave velocities are likely to decrease. In our experiments, the anomaly mainly occurs in the $I(\bar{1})$ stability fields irrespective of the existence of $P(\bar{1})$ structure.

Comparison with previous plagioclase studies

Previous determinations of elastic wave velocities of plagioclase at room temperature in the thermodynamically stability field are compared with our data (Figure 10). Ryzhova (1964) was the first to measure elastic wave velocities of plagioclase single crystals with various chemical compositions at room temperature and room pressure. These data suggest that velocities of plagioclase have a positive linear correlation with anorthite content. After that, Liebermann and Ringwood (1976) and Kono et al. (2008) measured the elastic wave velocities of polycrystalline plagioclase with An100 at 0.75 GPa and with An51 at 1 GPa, respectively, employing an ultrasonic pulse transmission technique using a piston cylinder apparatus without X-ray radiographic imaging. The data of Liebermann and Ringwood (1976) and Kono et al. (2008) do not agree with Ryzhova's data, and were faster. Liebermann and Ringwood (1979) speculated that Ryzhove had underestimated the data, possibly due to the presence of cracks, pores or inclusions in the single crystal measured at atmospheric pressure. Here, we point out another possibility that the velocities measured using piston cylinder apparatus had been the ones overestimated resulting, from overestimation of sample length because the sample lengths could not be measured directly in their studies. Higo et al. (2009) observed that sample length measured by X-ray radiographic imaging is shorter than that estimated from unit-cell volumes in high pressure for their cell assembly. Their observation indicates that the sample deforms not only through isotropic elastic deformation but also through plastic deformation owing to uniaxial compression of the sample by a hard buffer rod.

289 This implies that plagioclase sample lengths estimated in previous studies of plagioclase
290 possible to be overestimated if the samples were uniaxially compressed using a piston
291 cylinder apparatus. In contrast, sample lengths measured in our study are considered to be
292 accurate because they were measured directly using synchrotron X-ray radiography.

293 Our anorthite velocity data are compatible with the trends reported by Ryzhova
294 (1964), and are slower than that of Liebermann and Ringwood (1979). There are two factors
295 which may explain this inconsistency. One is the preferred orientation of the anorthite crystals,
296 which may have developed during the experiment. Anorthite has strong elastic anisotropy,
297 thus the ultrasonic measurements on a highly textured sample would not yield correct
298 aggregate velocities. In this study, the sample experienced not only isotropic elastic
299 deformation but also weak plastic deformation owing to uniaxial compression by a hard Al_2O_3
300 buffer rod. In order to eliminate this possibility, crystallographic orientation of the recovered
301 sample was measured by electron backscatter diffraction method. As a result, the preferred
302 orientation was not observed (Figure 11). Therefore, it is thought that lowering of velocity
303 accompanying elastic deformation had not occurred during the high pressure experiment. The
304 second is the presence of pores in the sintered polycrystalline anorthite during the
305 measurement of elastic wave velocities. Our sintered polycrystalline anorthite contained
306 ~1.2 % of pore before the experiments. After the experiments (Figure 1b), the pores were not
307 completely closed although they were considerably lessened (< ~0.5 %). To evaluate the
308 influence of pore on velocity lowering, we estimated elastic wave velocities of pore-free
309 polycrystalline sample using the theory of Takei (2002). Since the shape of pores was fairly
310 globular, calculation was performed assuming a dihedral angle of larger than 70°. The
311 calculated elastic wave velocities of a pore-free polycrystalline anorthite are very close to the
312 original data and are only higher than those of the pore-bearing sample by 0.4 % and 0.8 %

for V_S and V_P, respectively (Figure 10). It is concluded that the elastic wave velocities measured in our experiment is considered to be appropriate as aggregate velocities although it is slightly slower than the value of a sample without pores.

Implications for the crustal rocks in the subducting slab

Thin low-velocity layer having thickness of about several km has been observed in the upper portion of the subducting plate in the Japan arcs (e.g., Fukao et al. 1983; Hasegawa et al. 1994; Nakajima et al. 2009). It reaches depths of ~150 km (P = ~5 GPa) in central Japan and ~100 km (P = ~3 GPa) in northeast Japan, and disappears with increasing depths. Nakajima and his co-workers interpreted the low-velocity layer as a metamorphosed crust coexisting with interstitial aqueous fluid, because the observed V_P at depths of < 100 km in this layer is ~10% lower than that of fully-hydrous metamorphic MORB in blueshist facies (Shiina et al. 2013). This model is the basis for the hypothesis that subducting mafic rocks suffer complete metamorphic hydration before subduction. Plagioclase feldspars are one of most abundant minerals in gabbroic rocks that are subducted into the Earth's interior. Therefore the elastic anomaly in plagioclase has the potential to cause the low velocity anomaly in the slab in case of the cold slab in which the hydration reaction from gabbro to hydrous metamorphic rock is slow (Hasegawa et al. 1994). Our experimental results suggest that anorthite is metastable to at least less than 800 K and 7.0 GPa within the timescale of the experiments, although plagioclase will transform to a garnet-bearing assemblage at a depth of ~35 km when thermodynamic equilibrium is achieved at high temperature (>1300 K) (Green and Ringwood, 1967). Consequently, plagioclase may potentially survive in the slab to higher pressures if the slab is sufficiently cold.

Here, seismic velocities of gabbro and eclogite with NMORB composition were

337 calculated for the range of pressure and temperature assumed to be present in the subducting
338 slab. The one-dimensional geotherms along the slab-wedge interface for the central and
339 northeast Japan arcs were used as reference models for temperature (Iwamori, 2007). The
340 modal and chemical compositions of minerals were estimated using software for
341 thermodynamic calculation "PerpleX667" (Connolly 2012). The value of thermoelastic
342 parameters for coesite, kyanite, olivine, pyroxenes and garnet are after Hacker et al. (2003)
343 and Matsukage et al. (2005). The gabbro with MORB composition contains Na-bearing
344 plagioclase with An55-80. However the pressure dependence of the elastic wave velocity of
345 Na-bearing plagioclase has not been investigated. Therefore, the data of anorthite measured in
346 our experiment was used. Because the slab temperature is consistent with that of
347 high-temperature *I*(-1) stability field, we modelled temperature and pressure dependent elastic
348 wave velocities of anorthite with high-temperature *I*(-1) structure using a quadratic expression
349 with least squares fit: $V_X = a_0 + a_1T + a_2T^2 + bP$, where V_X (X = P, S), T and P is the wave
350 velocity, temperature and pressure. The parameters were determined to be a_0 = 6.407 km/s, a_1
351 = 1.085×10^{-3} km/s/K, a_2 = -5.630×10^{-7} km/s/K^2, b = -0.0280 km/s/GPa at V_P, and to be a_0 =
352 3.247 km/s, a_1 = 7.198×10^{-4} km/s/K, a_2 = -3.601×10^{-7} km/s/K^{2}and b = -0.0400 km/s/GPa at V_S.
353 Elastic wave velocities of An55 are estimated to be slower by ~5 % compared with that of
354 An100 (Figure 10). Since ~60 % of plagioclase is contained in the gabbroic rock, the
355 maximum bulk velocity lowering due to the compositional effect in plagioclase is estimated to
356 be ~3%. As shown in Figure 12, the observed V_S structures in the Japan arcs (Nakajima et al.
357 2009) are consistent with those of gabbro but lower than those of eclogite at a depth of < ~100
358 km. For central Japan, the V_P structure reported by Nakajima et al. (2009) is consistent with
359 the gabbro data. However, for northeast Japan, the eclogite velocities are more consistent with
360 the V_P by Nakajima et al. (2009). Nakajima et al. (2009) estimated the V_P structure by direct P

wave. Recently, the V_P structure was estimated by using P-to-S-converted wave, which is considered to be useful for the estimation of V_P structure at the upper portion of the subducting plate (Shiina et al. 2013). The data by P-to-S-converted wave is slower than the data by direct P wave. The V_P reported by Shiina et al. (2013) slightly lower than that of gabbro (Figure 12). The above comparison of the mineralogical model with existing seismic observations shows that the presence of metastable gabbro may reasonably explain observed low velocity in the slab without necessitating the introduction of hydration processes or a fluid phase. At present, it is difficult to determine whether the subducting crust is comprised of gabbroic or metamorphic mineral assemblies with aqueous fluid. Further studies are needed on elastic wave velocity measurements for Na-bearing plagioclase and on the reaction kinetics of metamorphic hydration of gabbro and gabbro-eclogite transition to address this issue.

Acknowledgments

We thank T. Ohuchi, M. L. Whitaker, S. Gréaux and K. Funakoshi for technical support in experiments. The comments made by anonymous reviewers are appreciated. This study was supported by the grant in aid for scientific research on innovative areas (21109004), and by Women's Future Development Center in Ehime University. The in situ experiments were performed at BL04B1 of Spring-8 (Proposal Nos. 2011A1362 and 2011B1365).

References

Angel, R.J. (1988) High-pressure structure of anorthite. American Mineralogist, 73, 1114-1119.

Angel, R.J. (1992) Order-disorder and the high-pressure $P(-1)$-$I(-1)$ transition in anorthite.

American Mineralogist, 77, 923-929.

Angel, R.J. (2004) Equation of state of plagioclase feldspars. Contribution to Mineralogy and Petrology, 146, 506-512.

Angel, R.J., Sochalski-Kolbus, L.M., and Tribaudino, M. (2012) Tilts and tetrahedra: the origin of the anisotropy of feldspars. American Mineralogist, 97, 765-778.

Birch, F. (1961) The velocity of compressional waves in rocks to 10 kilobars, Part 2. Journal of Geophysical Research, 66, 2199-2224.

Birch, F. (1963) Some geophysical applications of high-pressure research. *In Solids under Pressure, edited by W. Paul, and D. M. Warschauer*, pp. 137-162, McGraw Hill, New York.

Carpenter, M.A. (1991) Mechanisms and kinetics of Al-Si ordering in anorthite: II. Energetics and a Ginzburg-Landau rate law. American Mineralogy, 76, 1120-1133.

Christy, A.G., and Angel R.J. (1995) A Model for the origin of the cell-doubling phase transitions in clinopyroxene and body-centred anorthite. Physics and Chemistry of Minerals, *22*, 129-135.

Connolly, J.A.D. (2012) PerpleX667 report, http://www.perplex.ethz.ch/.

Connolly, J.A.D., and Kerrick, D.M. (2002) Metamorphic controls on seismic velocity of subducting oceanic crust at 100-250 km. Earth and Planetary Science Letters, *204*, 61-74.

Foit, F.F., and Peacor, D.R. (1973) The anorthite crystal structure at 410 and 830°C. American Mineralogist, *58*, 665-675.

Fukao, Y., Hori, S., and Ukawa, M. (1983) A seismological constraint on the depth of basalt-eclogite transition in a subducting oceanic crust. Nature, 303, 413-415.

Gibbs, G.V. (1982) Molecules as models for bonding in silicates. American Mineralogist, 67, 421-450.

Green, D.H. and Ringwood, A.E. (1966) An experimental investigation of the gabbro to

409 eclogite transformation and its petrological applications. Geochimica et Cosmochimica
410 Acta, 31, 767-833.
411 Hacker, B.R., Abers, G.A. and Peacock, S.M. (2003) Sunduction factory: 1. Theoretical
412 mineralogy, densities, seismic wave speeds, and H_2O contents. Journal of Geophysical
413 Research, 108, B1, 2029, doi:10.1029/2001JB001127.
414 Hackwell, T.P., and Angel, R.J. (1995) Reversed brackets for the *P*(-1)-*I*(-1) transition in
415 anorthite at high pressure and temperature. American Mineralogist, 80, 239-246.
416 Hasegawa, A., Horiuchi, S., and Umino, N. (1994) Seismic structure of the northeastern Japan
417 convergent margin: A synthesis. Journal of Geophysical Research, 99, 22295-22311.
418 Hays, J.F. (1966) Lime-alumina-shilica. Carnegie Inst. Washington Year Book, 65, 234-239.
419 Higo, Y., Kono, Y., Inoue, T., Irifune, T., and Funakoshi, K. (2009) A system for measuring
420 elastic wave velocity under high pressure and high temperature using a combination of
421 ultrasonic measurement and the multi-anvil apparatus at Spring-8. Journal of Synchrotron
422 Radiation, 16, 762-768, doi:10.1107/S0909049509034980.
423 Iwamori, H. (2007) Transportation of H_2O beneath the Japan arcs and its implications for
424 global water circulation. Chemical Geology, 239, 182-198.
425 Jamieson, J.C., Fritz, J.N., and Manghnani, M.H. (1982) Pressure measurement at high
426 temperature in x-ray diffraction studies: Gold as a primary standard. In High-Pressure
427 Research: Application to Earth and Planetary Sciences, Geophys. Monogr. Ser., vol. 67,
428 edited by S. Akimoto and M. H. Manghnani, pp. 27–48, Terra Sci., Tokyo.
429 Kono, Y., Miyake, A., Ishikawa, M., and Arima, M. (2008) Temperature derivatives of elastic
430 wave velocities in plagioclase (An50±1) above and below the order-disorder transition
431 temperature. American Mineralogist, 93, 558-564.
432 Koziol, A.M., and Newton, R.C. (1988) Redetermination of the anorthite breakdown reaction

and improvement of the plagioclase-garnet-Al_2SiO_5-quartz geobarometer. American Mineralogist, *73*, 216-223.

Kung, J., Li, B., Weidner, D.J., Zhang, J., Liebermann, R.C. (2002) Elasticity of $(Mg_{0.83}, Fe_{0.17})O$ ferropericlase at high pressure: ultrasonic measurements in conjunction with X-radiation techniques. Earth and Planetary Science Letters, 203, 557-566.

Li, B., Kung, J., and Liebermann, R.C. (2004) Modern techniques in measuring elasticity of Earth materials at high pressure and high temperature using ultrasonic interferometry in conjunction with synchrotron X-radiation in multi-anvil apparatus. Physics of the Earth and Planetary Interior, 143-144, 559-574.

Li, B., Liebermann, R.C., and Weidner, D.J. (1998) Elastic moduli of wadsleyite (β-Mg_2SiO_4) to 7 Gigapascals and 873 Kelvin. Science, 281, 675-677.

Liebermann, R.C., and Ringwood, A.E. (1976) Elastic properties of anorthite and the nature of the lunar crust. Earth and Planetaly Science Letters, 31, 69-74.

Matsukage, K.N., and Kawasaki, T. (2014) Hydrous origin of the continental cratonic mantle. Earth, Planets and Space, 66:29, doi:10.1186/1880-5981-66-29.

Matsukage, K.N., Nishihara, Y., and Karato, S. (2005) Seismological signature of chemical differentiation of Earth's upper mantle. Journal of Geophysical Research, 110, B12305, doi:10.1029/2004JB003504.

Nakajima, J., Tsuji, Y., and Hasegawa, A. (2009) Seismic evidence for thermally-controlled dehydration reaction in subducting oceanic crust. *Geophysical Research Letters, 36,* L03303, doi:10.1029/2008GL036865.

Newton, M.D., and Gibbs, G.V. (1980) *Ab initio* calculated geometries and charge distributions for H_4SiO_4 and $H_6Si_2O_7$ compared with experimental values for silicates and siloxanes. Physics and Chemistry of Minerals, *6*, 221-246.

457 Noritake, F., Kawamura, K., and Matsukage, K.N. (2013) Elastic anomalies of anorthite:
458 molecular dynamics simulation. Abstract of the meeting of *Japan Association of*
459 *Mineralogical Sciences*, *R2*, 14 (Japanese with English abstract).
460 Noritake, F., Kawamura, K., and Matsukage, K.N. (2014) Elastic wave velocity anomalies of
461 anorthite in subducting plate: molecular dynamics simulations. Submitted to Physics of the
462 Earth and Planetary Interior.
463 Ohuchi, T., Kawazoe, T., Nishihara, Y., Nishiyama, N., and Irifune, T. (2011) High pressure
464 and temperature fabric transitions in olivine and variations in upper mantle seismic
465 anisotropy. Earth and Planetary Science Letters, *304*, 55-63.
466 Prior, D., Boyle, A.P., Brenker, F., Cheadle, M., Day, A., Lopez, G., Peruzzo, L., Potts, G.J.,
467 Reddy, S., Spiess, R., Timms, N.E., Trimby, P., Wheeler, J., and Zetterström, L. (1999) The
468 application of electron backscatter diffraction and orientation contrast imaging in the SEM
469 to textural problems in rocks. American Mineralogist, 84, 1741-1759.
470 Redfern, S.A.T., Graeme-Barber, A., and Salje, E. (1988) Thermodynamics of plagioclase III:
471 Spontaneous Strain at the *I*(-1)-*P*(-1) phase transition in Ca-rich plagioclase. Physics and
472 Chemistry of Minerals, 16, 157-163.
473 Redfern, S.A.T., and Salje, E. (1987) Thermodynamics of plagioclase II: temperature
474 evolution of the spontaneous strain at the *I*(-1)-*P*(-1) phase transition in anorthite. Physics
475 and. Chemistry of Minerals, 14, 189-195.
476 Rondenay, S., Abers, G.A., and Van Keken, P.E. (2010) Seismic imaging of subduction zone
477 metamorphism. Geology, 36, 275-278.
478 Ryzhova, T.V. (1964) Elastic properties of plagioclase. Izv. Acad. Sci. USSR, Geophys. Ser, 7,
479 633-635.
480 Seront, B., Mainprice, D., and Christensen, N.I. (1993) A determination of the

three-dimensional seismic properties of anorthite: comparison between values calculated from the petrofabric and direct laboratory measurements. Journal of Geophysical Research., 98, 2209-2221.

Shiina, T., Nakajima, J., and Matsuzawa, T. (2013) Seismic evidence for high pore pressures in the oceanic crust: Implications for fluid-related embrittlement. *Geophysical Research Letters*, 40, doi: 10.1002/grl.50468.

Takei, Y. (2002) Effect of pore geometry on V_P/V_S: from equilibrium geometry to crack. Journal of Geophysical. Research, 107, doi:10.1029/2001JB000522.

Tribaudino, M., and Angel, R.J. (2012) The thermodynamics of the I(-1)-P(-1) phase transition in Ca-rich plagioclase from an assessment of the spontaneous strain. Physics and Chemistry of Minerals, doi:10.1007/s00269-012-0524-x.

Tribaudino, M., Bruno, M., Nestola, F., Pasqual, D., and Angel, R.J. (2011) Thermoelastic and thermodynamic properties of plagioclase feldspars from thermal expansion measurements. American Mineralogist, 96, 992-1002.

Utsumi, W., Funakoshi, K., Urakawa, S., Yamakata, M., Tsuji, K., Konishi, H., Shimomura, O. (1998) Spring-8 beam lines for high pressure science with multi-anvil apparatus. Review of High Pressure Science Technique. 7, 1484–1486.

Von Dreele, R.B., and Larson, A.C. (2001) GSAS (General Structure Analysis System). Copyright, Regents of the University of California.

Wang, H., Todd, T., Richter, D., and Simmons, G. (1973) Elastic properties of plagioclase aggregates and seismic velocities in the moon. Proceedings of the Fourth Lunar Science Conference, 3, 2663-2671.

Weidner, D.J., Wang, H., and Ito, J. (1978) Elasticity of orthoenstatite. Physics of the Earth and Planetary Interior, 17, 7-13

505

506 **Figure captions**

507 Figure 1. Orientation contrast images of the synthesized polycrystalline anorthite taken using
508 forescatter detectors in scanning electron microprobe equipped with field emission gun
509 (FE-SEM) with the polished sample inclined at 70° (Prior et al. 1999). a) Before experiment,
510 b) after experiment. Bright particles in (b) are reaction products at high pressure.

511

512 Figure 2. A schematic illustration of cell assembly for elastic wave velocity measurements.

513

514 Figure 3. A typical example of the X-ray radiographic image (a) and the ultrasonic signals (b
515 and c) at 1373 K and 1.2 GPa. R1, R2 and R3 are shown in Figure 2.

516

517 Figure 4. Experimental pressure and temperature paths in elastic wave velocity measurements
518 on anorthite. Open diamonds denote the preheating stage. Phase relations of anorthite are after
519 Hackwell and Angel (1995) and Koziol and Newton (1988). The pressure of the phase
520 transition from P(-1) to high-pressure I(-1) was dependent on the state of Si and Al order, and
521 when Q_{OD} (see text) decreases from 0.92 to 0.78, the pressure of the phase transition increases
522 from 2.5 GPa to 4.8 GPa (Angel, 1992). Open circles indicate the pressure and temperature
523 conditions corresponding to the temperature-induced kink in velocities.

524

525 Figure 5. Variations in V_P (a-c), V_S (d-f) of cycles (2)-(8) as a function of temperature. Error of
526 velocities is listed in Table 1.

527

528 Figure 6. Variations in a) V_P, and b) V_S as a function of pressure at temperatures of 300-773 K.

529 Error of velocities is listed in Table 1.

530

531 Figure 7. A typical diffraction pattern for anorthite at room temperature and room pressure.

532

533 Figure 8. Unit cell parameters of anorthite as a function of temperature. Error of the unit cell
534 parameters (one standard deviation) is smaller than symbols.

535

536 Figure 9. Unit cell volume of anorthite as a function of pressure. Error of the unit cell volume
537 (one standard deviation) is smaller than symbols.

538

539 Figure 10. Elastic wave velocities of plagioclase with various chemical compositions at room
540 temperature and at pressures of $\leq$1 GPa. The Ryzhova's data are Voigt-Reuss-Hill averages of
541 single crystals. Gray circles show the velocities after correction for pore effect.

542

543 Figure 11. Pole figures showing crystallographic orientations of anorthite grains in recovered
544 sample from S2708 (equal area lower hemisphere projections of [100] and [(-1)00] directions,
545 (010) and (001) planes). The orientations of grains were measured by electron backscatter
546 diffraction method using FE-SEM (Ohuchi et al. 2011). 404 measurements are used. The
547 cylinder axis is vertical.

548

549 Figure 12. Comparison of V_P and V_S in the crustal portion of the subducting slab in the Japan
550 arcs with those of gabbro and eclogite. Solid circles show V_P and V_S values along A-A' and
551 B-B' sections of northeastern and central Japan of Nakajima et al. (2009). Open diamonds
552 denote averaged V_P in northeastern Japan estimated using P-to-S-converted waves (Shiina et

553 al. 2013)

554

Table 1. Experimental conditions, density, elastic wave velocities and elastic parameters for anorthite

Temperature (K)	Load (ton)	Pressure (GPa)	V_P (km/s)	V_S (km/s)	ρ (g/cm^3)	K_S (GPa)	G (GPa)
Run No. S2708							
before experiment							
300	0	0.0001			2.754		
heating (2)							
1373	150	1.21(10)	6.81(1)	3.51(1)	2.765	82.6(4)	34.1(2)
1273	150	1.09(7)	6.85(1)	3.54(<1)	2.765	83.6(3)	34.6(1)
1173	150	1.07(8)	6.87(1)	3.55(1)	2.767	84.1(7)	34.8(1)
1073	150	0.99(13)	6.89(1)	3.56(1)	2.768	84.4(4)	35.2(2)
973	150	0.95(11)	6.90(2)	3.57(1)	2.769	85.1(7)	35.2(1)
873	150	0.90(9)	6.90(<1)	3.57(1)	2.770	84.9(2)	35.3(1)
773	150	0.82(8)	6.89(1)	3.56(1)	2.771	84.8(4)	35.1(2)
673	150	0.75(9)	6.87(<1)	3.55(1)	2.772	84.2(2)	34.8(2)
573	150	0.66(10)	6.82(1)	3.51(1)	2.773	83.5(3)	34.2(2)
473	150	0.67(7)	6.81(1)	3.48(<1)	2.775	84.0(4)	33.7(1)
373	150	0.62(7)	6.95(<1)	3.66(1)	2.777	84.5(2)	37.3(1)
300	150	0.63(4)	7.01(1)	3.73(<1)	2.778	84.9(4)	38.6(1)
heating (3)							
773	220	2.83(6)	6.84(3)	3.47(1)	2.847	87.7(11)	34.3(2)
673	220	2.82(9)	6.79(3)	3.45(1)	2.850	86.3(10)	33.8(1)
573	220	2.67(10)	6.83(3)	3.46(<1)	2.853	87.6(12)	34.1(1)
473	220	2.62(4)	6.88(3)	3.51(1)	2.855	88.4(12)	35.2(1)
373	220	2.56(6)	6.95(2)	3.60(1)	2.857	88.6(9)	37.1(3)
300	220	2.53(2)	7.00(1)	3.66(1)	2.858	88.8(6)	38.4(2)
heating (4)							
773	250	3.79(18)	6.81(1)	3.44(1)	2.879	88.0(4)	34.1(2)
673	250	3.71(7)	6.80(1)	3.44(<1)	2.880	87.8(4)	34.1(<1)
573	250	3.63(8)	6.83(1)	3.46(<1)	2.882	88.5(5)	34.5(1)
473	250	3.60(4)	6.90(3)	3.53(<1)	2.884	89.2(10)	36.0(<1)
373	250	3.54(3)	6.95(2)	3.61(<1)	2.885	89.5(9)	37.6(<1)

300	250	3.53(4)	7.00(1)	3.65(1)	2.885	90.1(5)	38.4(2)
heating (5)							
773	280	4.55(14)	6.78(1)	3.41(1)	2.898	88.2(5)	33.7(2)
673	280	4.42(8)	6.78(3)	3.42(1)	2.898	88.0(13)	33.9(2)
573	280	4.35(7)			2.900		
473	280	4.26(3)	6.89(2)	3.53(1)	2.902	89.5(9)	36.1(1)
373	280	4.28(1)	6.95(7)	3.61(2)	2.902	89.8(28)	37.7(4)
302	280	4.24(4)	6.97(1)	3.64(1)	2.903	89.7(6)	38.4(2)
573	280	4.45(6)	6.82(2)	3.46(1)	2.902	88.9(7)	34.7(1)
300	280	4.37(4)	6.96(2)	3.64(1)	2.907	89.7(8)	38.4(2)
heating (6)							
773	320	5.05(4)	6.74(2)	3.39(1)	2.922	88.1(7)	33.6(1)
673	320	4.84(7)	6.77(2)	3.41(1)	2.921	88.6(7)	34.1(1)
573	320	4.76(9)	6.82(2)	3.46(1)	2.923	89.2(8)	35.0(1)
473	320	4.71(5)	6.87(2)	3.53(1)	2.923	89.5(9)	36.4(2)
373	320	4.68(1)	6.92(2)	3.59(1)	2.923	89.7(10)	37.7(2)
300	320	4.64(9)	6.94(3)	3.63(1)	2.926	89.7(12)	38.5(2)
heating (7)							
773	390	5.66(14)	6.72(1)	3.38(1)	2.944	88.2(4)	33.6(1)
673	390	5.60(3)	6.75(2)	3.41(<1)	2.943	88.6(6)	34.2(1)
573	390	5.52(5)	6.81(2)	3.47(1)	2.944	89.5(7)	35.4(2)
473	390	5.33(2)	6.86(3)	3.53(1)	2.945	89.9(12)	36.6(3)
373	390	5.15(7)	6.89(2)	3.58(1)	2.944	89.7(9)	37.6(2)
300	390	5.00(35)	6.92(1)	3.61(1)	2.948	89.9(6)	38.4(2)
heating (8)							
773	480	6.99(1)	6.67(1)	3.36(<1)			
673	480	6.71(12)	6.70(1)	3.40(1)	2.988	88.4(5)	34.5(1)
573	480	6.59(13)	6.77(2)	3.46(1)	2.988	89.4(7)	35.7(2)
473	480	6.60(3)	6.81(2)	3.51(1)	2.989	89.5(10)	36.8(2)
373	480	6.51(8)	6.84(2)	3.55(1)	2.989	89.6(10)	37.7(1)
300	480	6.52(3)	6.86(2)	3.57(1)	2.991	89.7(9)	38.2(1)

Numbers in parentheses are the one standard deviation (1σ) in the last digit. 1σ of density is less than 0.001 (g/cm^3)

555

556

557

558

559

560 **APPENDIX**

561 The in situ elastic wave velocity measurements of anorthite were performed twice. In first
562 experiments (S2646), the measurements were carried out under load of 150 ton and 250 ton
563 after preheating process. We, however, could not obtain reliable temperature and pressure data
564 at except for room temperature because thermocouple was broken during preheating process.
565 In second experiment (S2708), we succeeded to measure the temperature directly by
566 thermocouple, and the reliable data in wide pressure and temperature range were corrected
567 (see text). Therefore, only the second experiment was used for the discussion. Here, in order
568 to prove reproducibility of the elastic wave velocity anomalies observed by S2708, the results
569 of S2646 are compared. Temperature in S2646 was estimated using relation between
570 temperature and electric power at the same loads in S2708. In S2646, pressures at room
571 temperature after heating was calculated from the EOS of MgO as 1.5 GPa for 150 ton and
572 3.1 GPa for 250 ton, respectively. The pressure at 150 tons was higher than that of 150 tons of
573 S2708, and, in the case of 250 tons, it becomes lower. Therefore there may be larger
574 uncertainty in this temperature estimation. As shown in Figure A1, the elastic wave velocity
575 anomalies were evident in the experiment of S2646. The variation of V_P of S2646 agrees well
576 with that of S2706. In the experiments at 150 ton, the V_S of S2646 becomes slower than that
577 of S2708. The lower V_S in S2646 are considered to originate from the difference in pressure
578 because the dV_S/dP shows a negative though dV_P/dP is constant at below ~4 GPa. In
579 conclusion, these comparisons demonstrate the reproducibility of our experiments.

580

581 Figure A1. Elastic wave velocities as a function of temperature in S2646 and S2708.

582

583

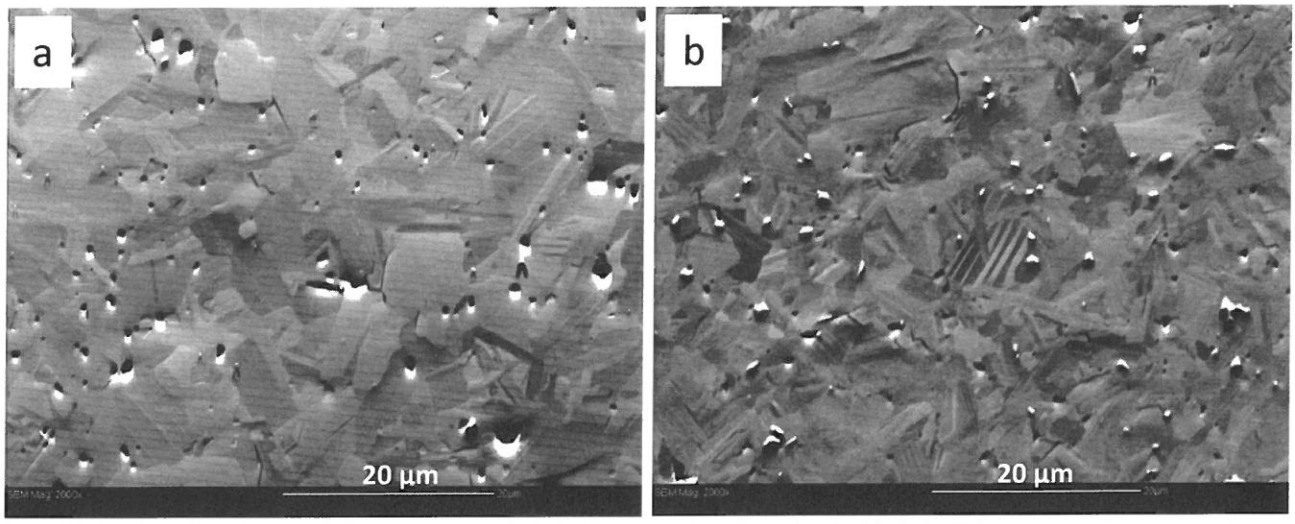

Figure 1. Orientation contrast images of the synthesized polycrystalline anorthite taken using forescatter detectors in scanning electron microprobe equipped with field emission gun (FE-SEM) with the polished sample inclined at 70 ° (Prior et al., 1999). a) Before experiment, b) after experiment. Bright particles in (b) are reaction products at high pressure.

Matsukage et al.

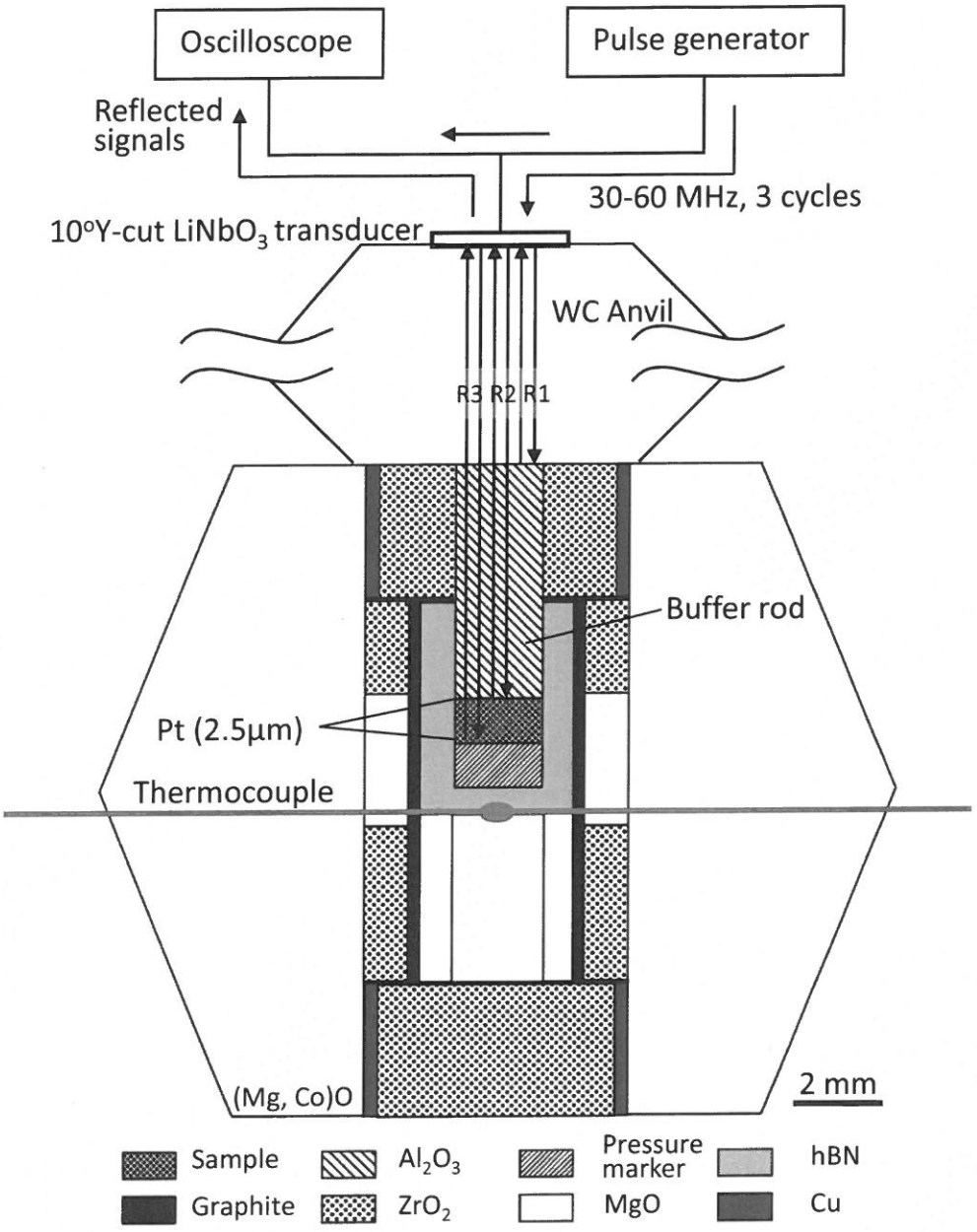

Figure 2. A schematic illustration of cell assembly for elastic wave velocity measurements.

Matsukage et al.

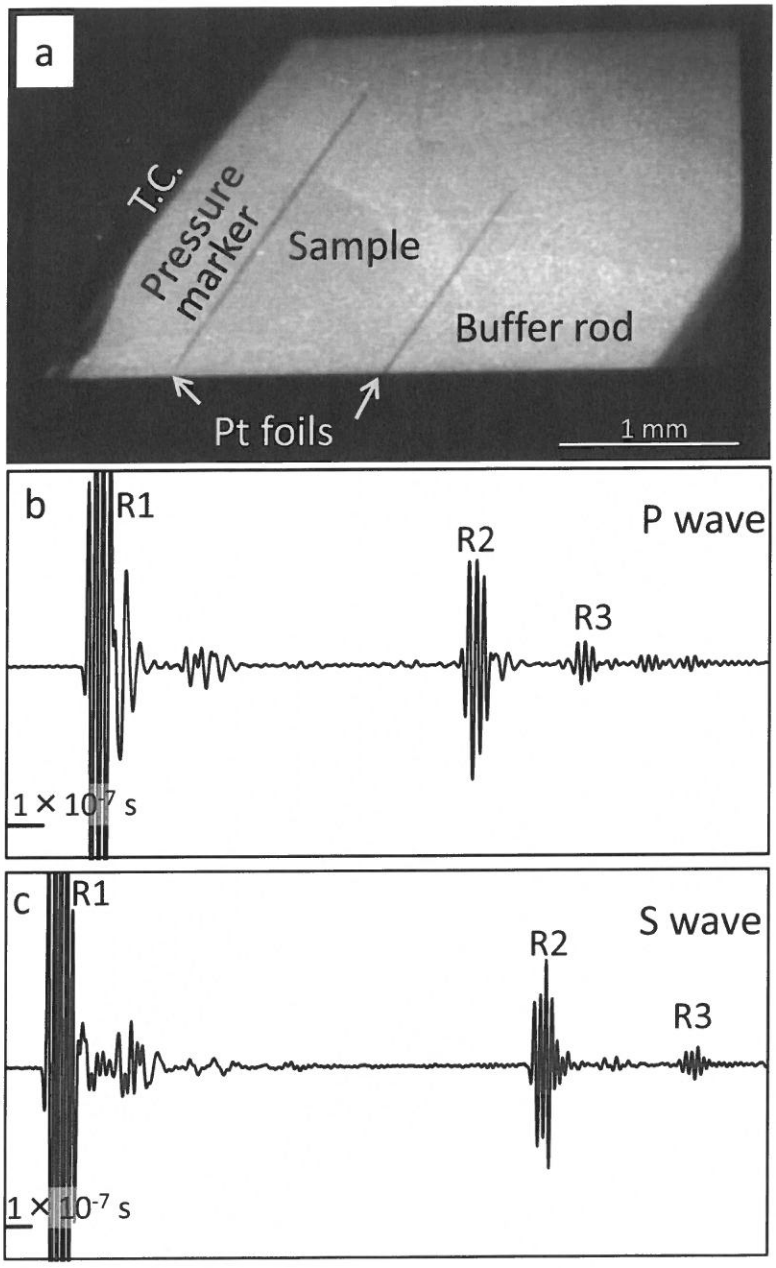

Figure 3. A typical example of the X-ray radiographic image (a) and the ultrasonic signals (b and c) at 1373 K and 1.2 GPa. R1, R2 and R3 are shown in Figure 2.

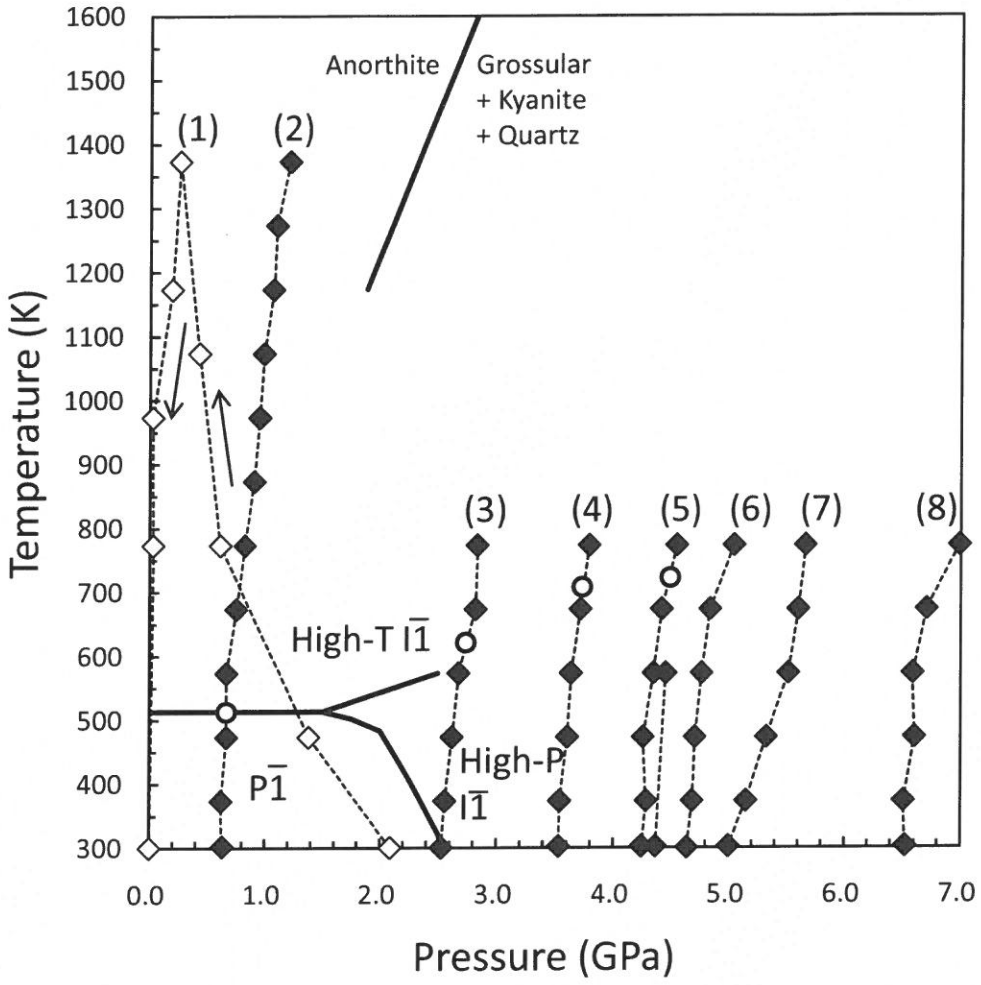

Figure 4. Experimental pressure and temperature paths in elastic wave velocity measurements on anorthite. Open diamonds denote the preheating stage. Phase relations of anorthite are after Hackwell and Angel (1995) and Koziol and Newton (1988). The pressure of the phase transition from P(-1) to high-pressure I(-1) was dependent on the state of Si and Al order, and when Q_{OD} (see text) decreases from 0.92 to 0.78, the pressure of the phase transition increases from 2.5 GPa to 4.8 GPa (Angel, 1992). Open circles indicate the pressure and temperature conditions corresponding to the temperature-induced kink in velocities.

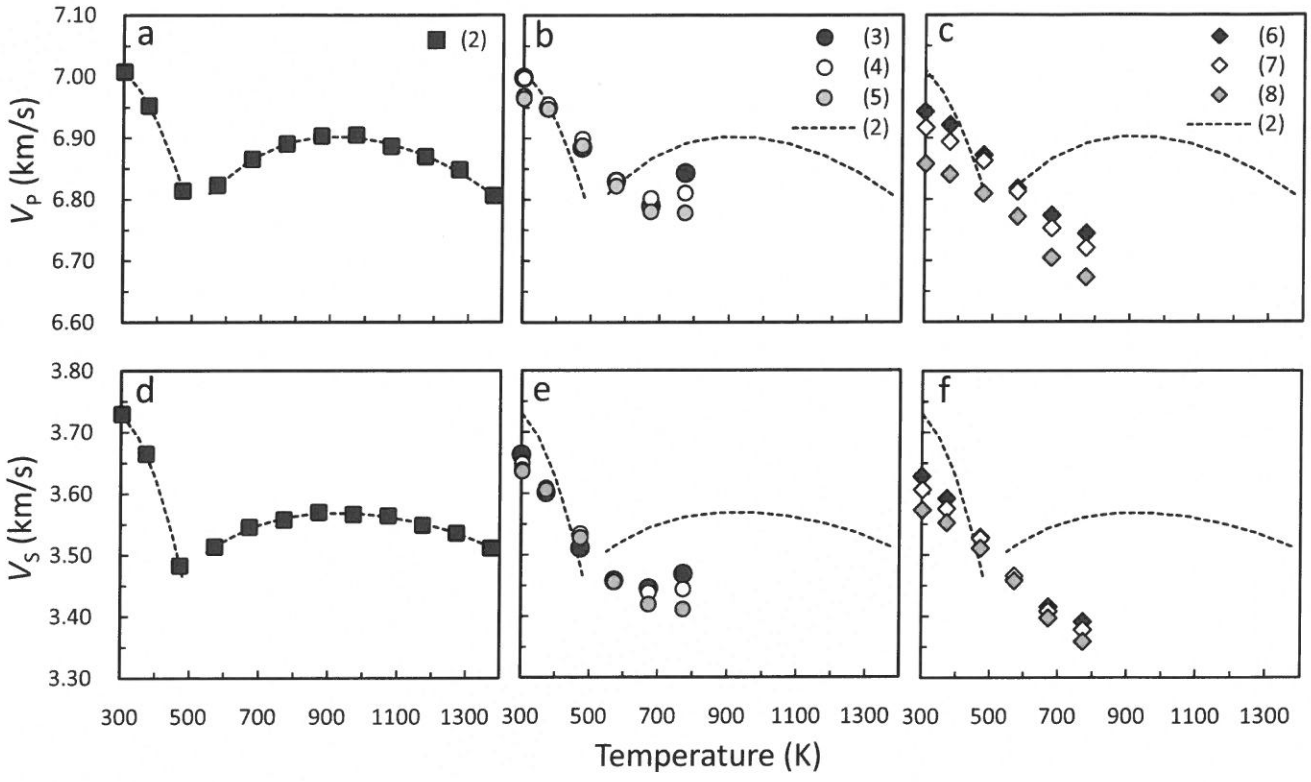

Figure 5. Variations in V_P (a-c), V_S (d-f) of cycles (2)-(8) as a function of temperature. Error of velocities is listed in Table 1.

Matsukage et al.

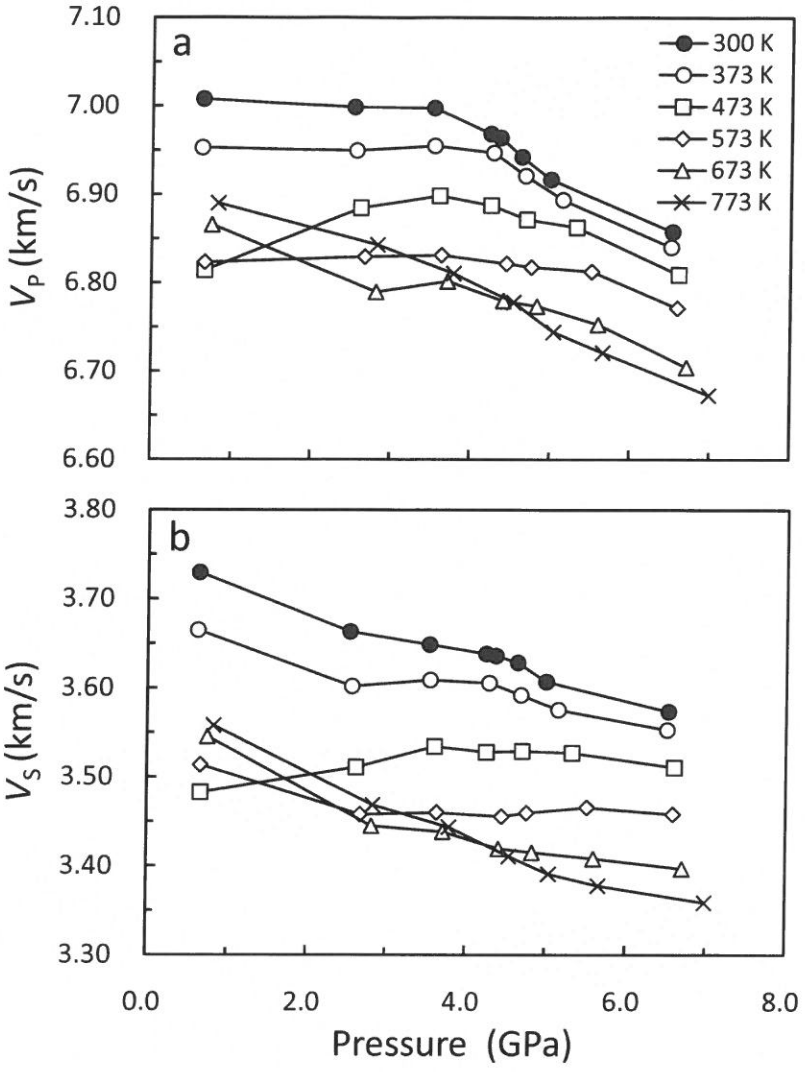

Figure 6. Variations in a) V_P, and b) V_S as a function of pressure at temperatures of 300-773 K. Error of velocities is listed in Table 1.

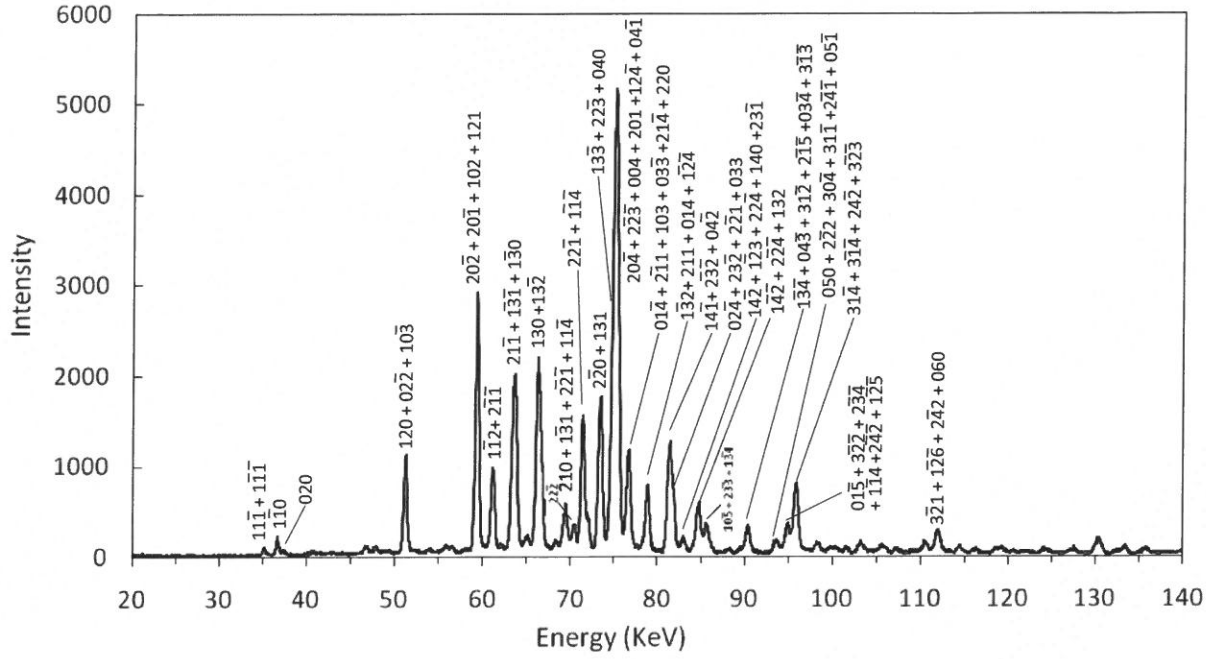

Figure 7. A typical diffraction pattern for anorthite at room temperature and room pressure.

Matsukage et al.

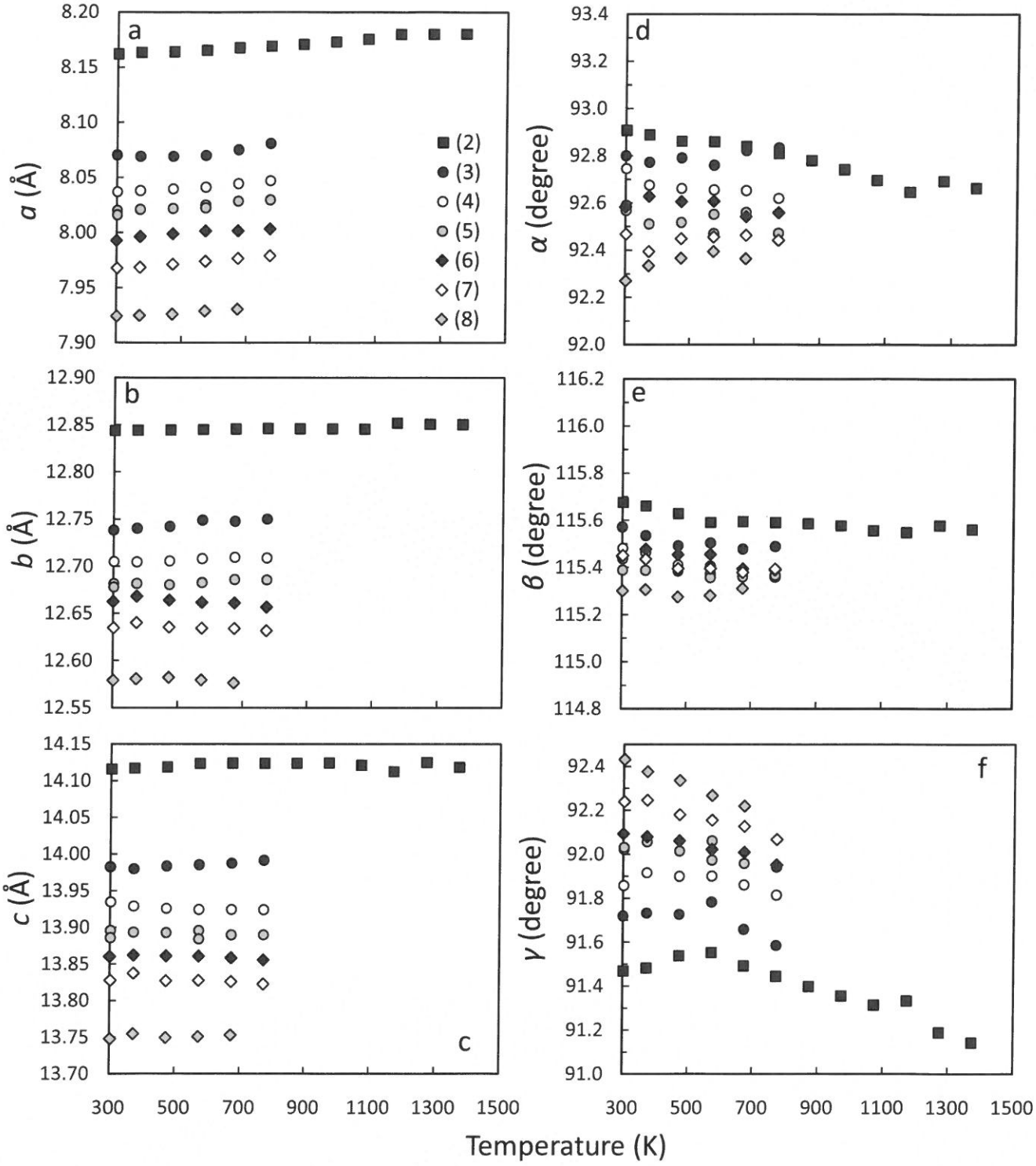

Figure 8. Unit cell parameters of anorthite as a function of temperature. Error of the unit cell parameters (one standard deviation) is smaller than symbols.

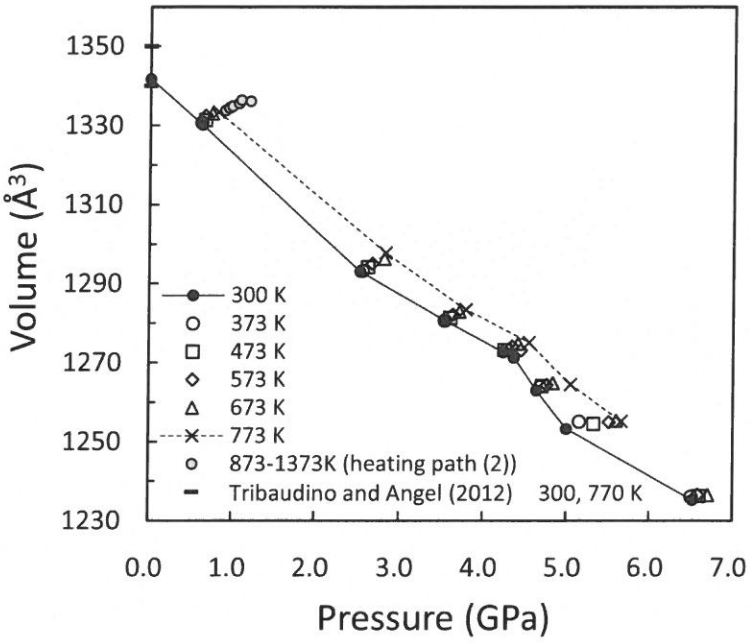

Figure 9. Unit cell volume of anorthite as a function of pressure. Error of the unit cell volume (one standard deviation) is smaller than symbols.

Matsukage et al.

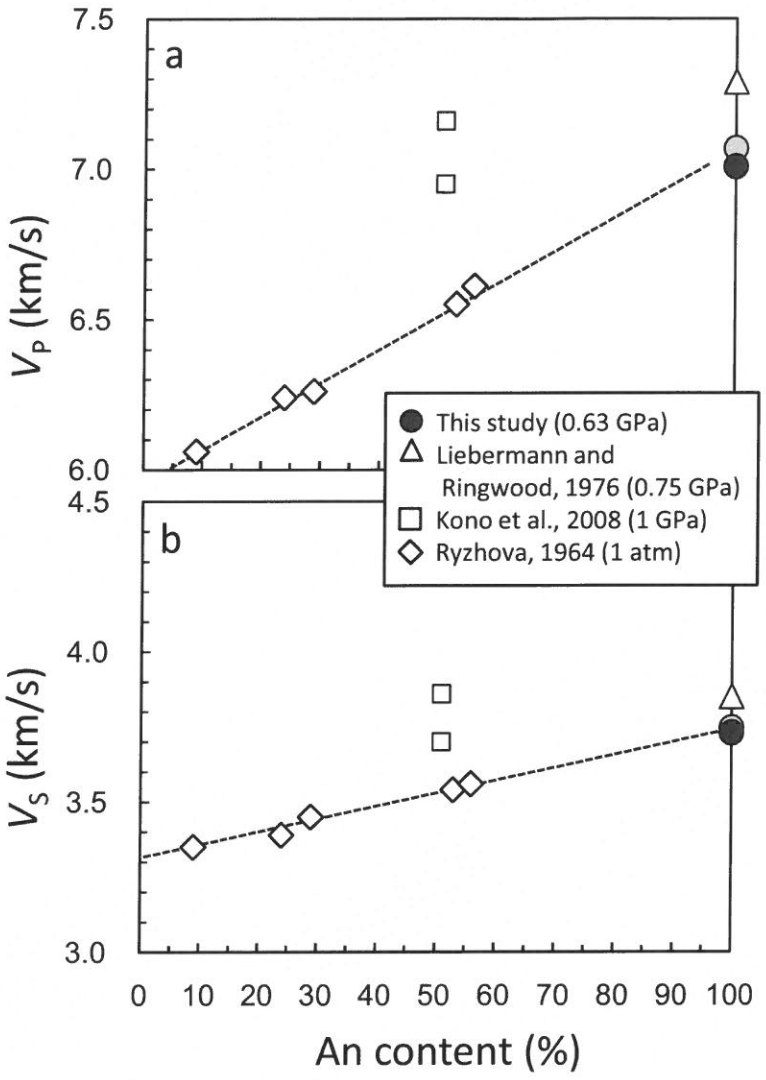

Figure 10. Elastic wave velocities of plagioclase with various chemical compositions at room temperature and at pressures of ≤1 GPa. The Ryzhova's data are Voigt-Reuss-Hill averages of single crystals. Gray circles show the velocities after correction for pore effect.

Matsukage et al.

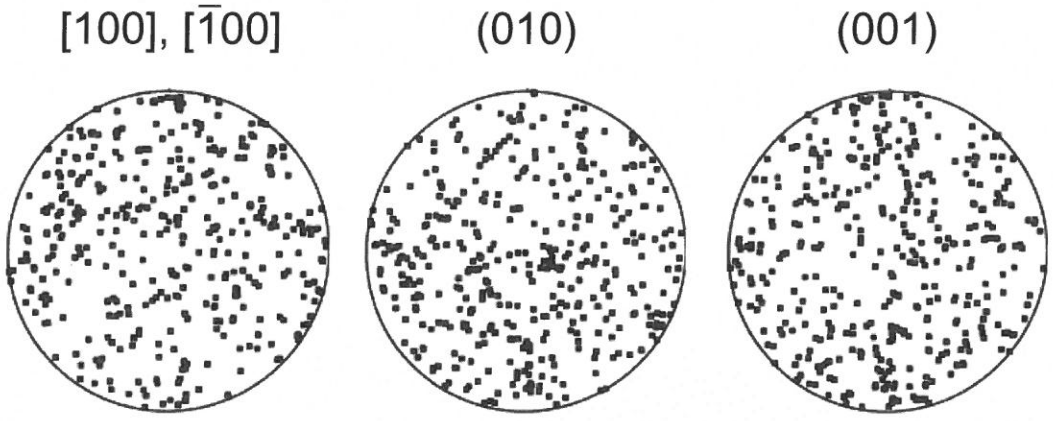

Figure 11. Pole figures showing crystallographic orientations of anorthite grains in recovered sample from S2708 (equal area lower hemisphere projections of [100] and [(-1)00] directions, (010) and (001) planes). The orientations of grains were measured by electron backscatter diffraction method using FE-SEM (Ohuchi et al. 2011). 404 measurements are used. The cylinder axis is vertical.

Matsukage et al.

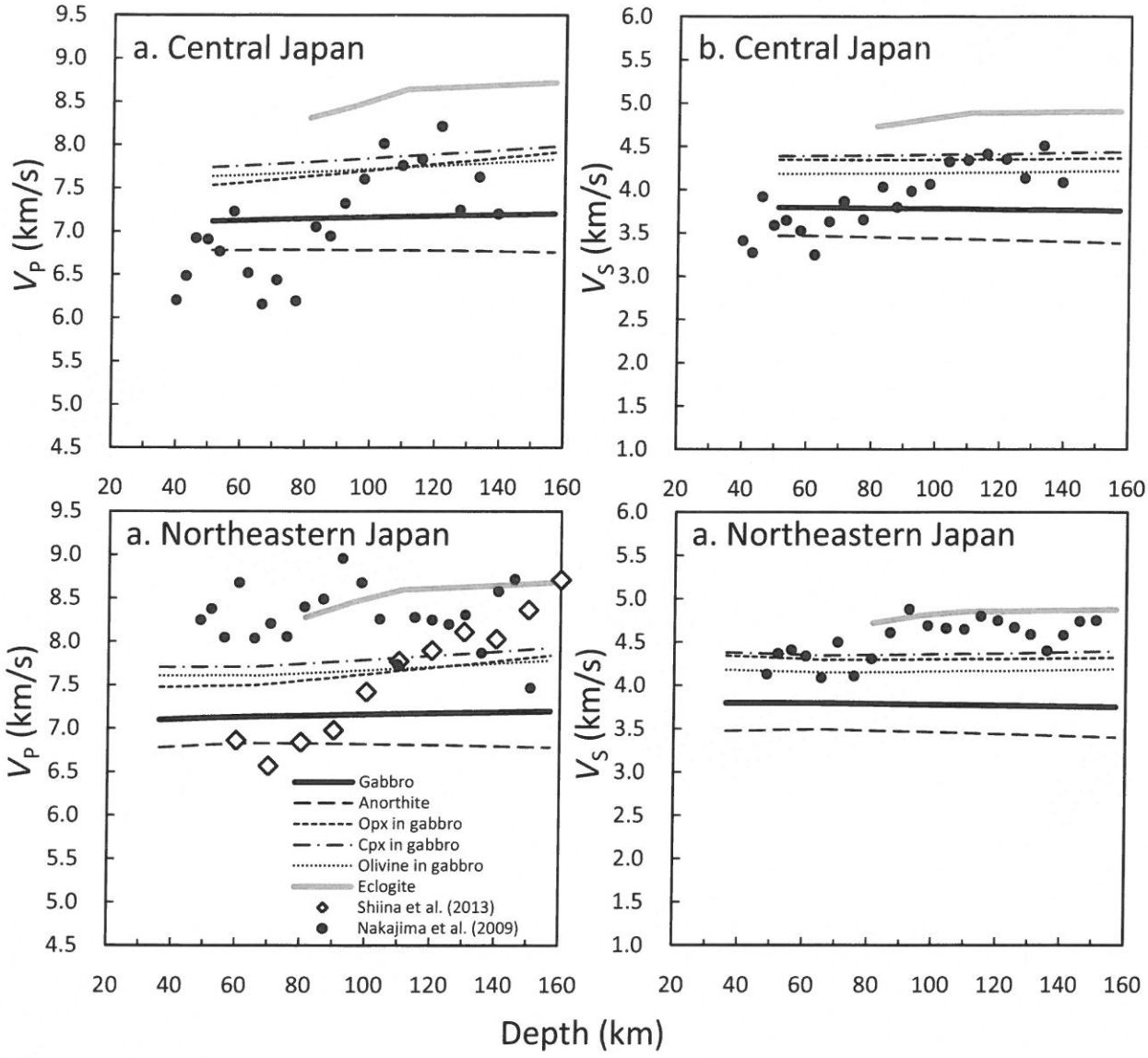

Figure12. Comparison of V_P and V_S in the crustal portion of the subducting slab in the Japan arcs with those of gabbro and eclogite. Solid circles show V_P and V_S values along A-A' and B-B' sections of northeastern and central Japan of Nakajima et al. (2009). Open diamonds denote averaged V_P in northeastern Japan estimated using P-to-S-converted waves (Shiina et al. 2013).

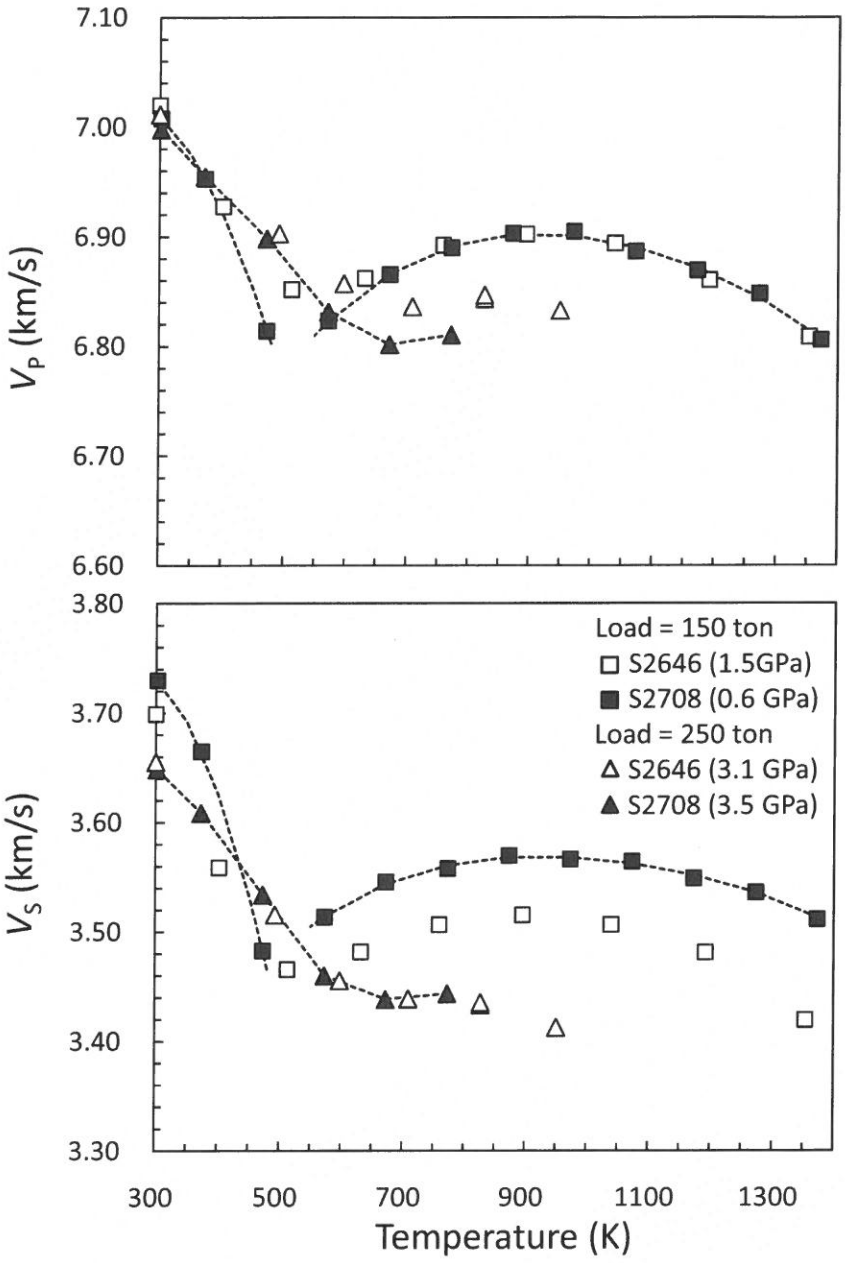

Appendix

Figure A1. Elastic wave velocities as a function of temperature in S2646 and S2708.

Matsukage et al.